

## **Tide–surge interaction at the head of the Bay of Bengal during Cyclone Aila**

**Charls Antony<sup>1,\*</sup>, A. S. Unnikrishnan<sup>1</sup>, Y. Krien<sup>2,3</sup>, P. L. N. Murty<sup>4</sup>, S. V. Samiksha<sup>5</sup>, A. K. M. S. Islam<sup>6</sup>**

<sup>1</sup>Formerly, CSIR – National Institute of Oceanography, Dona Paula, Goa 403004, India

<sup>2</sup>Laboratoire d'études en Géophysique et Océanographie Spatiales (LEGOS), Toulouse, France

<sup>3</sup>Littoral Environnement et Sociétés (LIENS), La Rochelle, France

<sup>4</sup>ESSO – Indian National Centre for Ocean Information Services, Hyderabad, India

<sup>5</sup>CSIR – National Institute of Oceanography, Dona Paula, Goa 403004, India

<sup>6</sup>Institute of Water and Flood Management, Bangladesh University of Engineering and Technology, Dhaka, Bangladesh

\*Corresponding author

Email: antonyocharlz@gmail.com

### **Abstract**

Tide–surge interaction serves a critical role in shallow coastal regions in modifying the characteristics of peak water levels during storm events. In the present study, we investigated the tide–surge interaction in the coastal waters at the head of the Bay of Bengal (BoB) during Cyclone Aila, a Category 1 cyclone. The space–time characteristics of the interaction were discussed. The numerical simulation results reveal that the interaction was significant with interaction heights of up to 1 m at many locations that were even a few hundred kilometres away from the maximum surge. The spatial pattern of the interaction exhibited lower values in the central part of the head of the BoB due to the reduction in the width of the continental shelf and the relatively lower tidal amplitudes in this region compared with those in the remaining portion of the head of the BoB. The overall effect of the interaction was the reduction in the peak water levels. Favourable factors such as the extreme shallowness of the coastal waters, tidal contribution, and complex coastline geometry explain the strong tide–surge interaction at the head of the BoB.

**Keywords:** Tide; Storm surge; Tide–surge interaction; ADCIRC; Cyclone Aila; Bay of Bengal

## 1. Introduction

The tropical cyclones over the BoB have gained much attention due to the severe impacts caused by storm surges associated with them. Some of the past cyclone events have caused massive loss of life and property in the coastal regions surrounding the BoB (Frank and Husain, 1971; Frintzet *al.*, 2009), which are densely populated. The storm surges in the BoB are larger compared to those in other regions. Five storm surges of  $\geq 5$  m occur on an average in the BoB every decade (Needhamet *al.*, 2015). The converging characteristic of the coastline and the shallow and broad continental shelf in the northern BoB serve a significant role in amplifying the storm surges (Flierl and Robinson, 1972). The inland reach of the surges is high due to the low-lying characteristic of the coast and the presence of numerous estuarine channels (Johns and Ali, 1980). The total water level should be forecasted to reduce the risks related to storm surges. Because the total water level is a combination of tides and surges, the phase of the tidal cycle serves a critical role in determining the total surge impact. Semi-diurnal tides undergo amplification on the wide shelf off the head of the BoB (Sindhu and Unnikrishnan, 2013). The nonlinear interaction between a tide and surge forms a critical element that can be used to predict the accurate total water level in this region owing to the shallow water depths and tidal amplitudes that reach up to several metres, especially during spring tides.

Tide–surge interaction is found to be significant in shallow seas and estuaries (Prandle and Wolf, 1978). A significant amount of interaction causes noticeable changes in the tide and surge characteristics, for example, changes in the surge magnitude and duration (As-Salek and Yasuda, 2001). Such interaction studies have originated from the studies conducted in the Thames Estuary, a region where the tide–surge interaction is quite prominent. The pioneering studies pertaining to observe and understand tide–surge interaction include those of Doodson (1929) and Proudman (1955). By using surge observations obtained from Southend, U.K., Doodson (1929) revealed that surge peaks were frequent on rising tides and that surges were larger during low tide than those during high tide. Rossiter (1961) statistically found significant tide–surge interactions by using the storm surge observations of the Thames Estuary. According to him, interaction tends to amplify the surge heights on the rising tide. He suggested a mutual phase alteration between tide and surge as the physical interaction mechanism. Later, Horsburgh, and Wilson (2007) proposed a simple mathematical explanation for the surge clustering on the rising tide observed along the east coast of the United Kingdom. They suggested that the phase modification of a tide signal due to a surge and a tide-modulated surge generation are the two processes which contribute to the surge clustering on the rising tide. Tide–surge interaction has been studied in many other coastal regions, such as the Gulf of

Mexico (Rego and Li, 2010), seas around the Korean Peninsula (Park and Suh, 2012), the east coast of the USA (Fenget *al.*, 2016), and the South China Sea (Zhanget *al.*, 2017).

In the case of the 1970 Bhola cyclone that occurred in the BoB, Daset *al.* (1974) noted an overestimation of the total water levels (approximately 1 m) when the tides and surges were added linearly compared with the total water levels obtained by including the coupled effect of tides and surges. Subsequently, Johns and Ali (1980) found that compared with the surge heights that do not include tide–surge interaction, the heights that includes the tide–surge interaction were lower during a high tide and higher during a low tide. Antony and Unnikrishnan (2013) analysed hourly tide-gauge data of approximately 27 years and noted a frequent occurrence of surge peaks away from high tide at Hiron Point, a station situated at the head of the BoB. They studied a characteristic surge distribution due to tide–surge interaction. By studying two major cyclones which made landfall on the coastal region in Bangladesh, Hussain and Tajima (2017) concluded that during ebb tides the total water level, including the tide–surge interaction, was higher than that from a linear addition of tide and surge, whereas the opposite was noticed during high tide. By investigating storm surges during Cyclone Sidr, Krienet *al.* (2017) presented that the tide–surge interaction changed the total water levels by more than 1 m close to the landfall area, which was located in the rivers and in the northeastern part of the head of the BoB.

A few studies have attempted to simulate the storm surge during Cyclone Aila (Paul *et al.*, 2016; Gayathri *et al.*, 2016). Although these studies have used coupled tide–surge models, their primary interests were towards coastal inundation (Gayathri *et al.*, 2016) and air bubble effects (Paul *et al.*, 2016) that were observed during the event. In the present study, we investigated the space–time characteristics of the tide–surge interaction during Cyclone Aila through a numerical modelling approach.

## **2. Cyclone Aila**

Cyclone Aila was developed from a tropical disturbance that formed over the central BoB. The disturbance strengthened into a tropical storm at 88.5° E and 17.7° N (Figure 1a) at 00:00 UTC on 24 May 2009. Subsequently, the storm advanced northwards and crossed the land near Sagar Island (Figure 1a) after 06:00 UTC on 25 May. Before its landfall, the storm intensified into a Category 1 cyclone with a maximum sustained wind speed of up to 65 kt (Joint Typhoon Warning Centre (JTWC) tropical cyclone best-track data) (Figure 1b). The minimum pressure at the centre of the cyclone was approximately 974 mb (Figure 1b). The storm surge during the event attained heights of

approximately 3m (IFNet 2009; Roy *et al.* 2009) and caused major damage along the northeastern and southwestern coastal regions of India and Bangladesh.

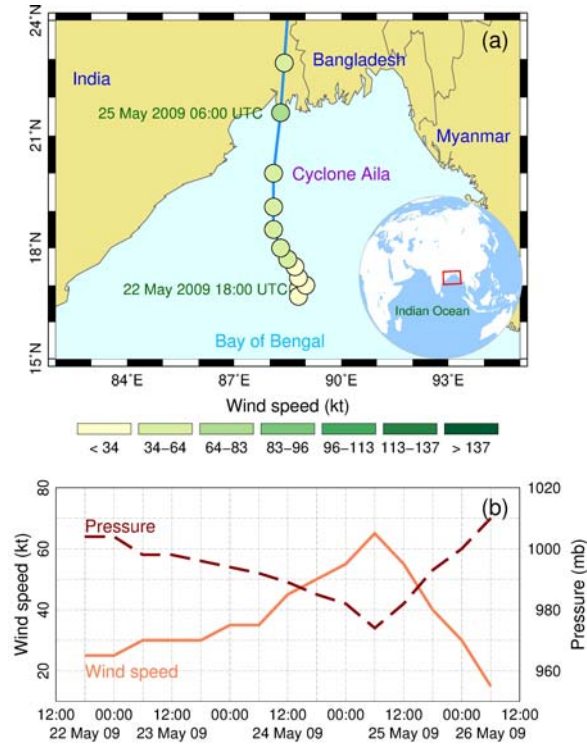


**Figure 1.** (a) Track of Cyclone Aila with its maximum surface (10 m) wind speed presented using the Saffir–Simpson hurricane wind scale. (b) Time evolution of the six hourly maximum wind speed and minimum mean sea-level pressure during the cyclone. The cyclone data source: JTWC tropical cyclone best-track data.

### 3. Hydrodynamic model

The advanced circulation (ADCIRC) model (Luettich *et al.*, 1992; Luettich and Westerink, 2004; Dawson *et al.*, 2006), which solves vertically integrated shallow-water equations for water-surface elevations and currents, was used in the present study. The model uses triangular elements of various size, thus allowing the use of a finer resolution near the coast and a coarser resolution in the open ocean. ADCIRC has a wide range of applications, including modelling of tides, storm surges, and coastal inundation. The model has been successfully used for various applications in the BoB, such as tidal characteristics (Rose and Bhaskaran 2017), wave–current interaction (Samiksha *et al.*, 2017), and coastal inundation (Rao *et al.*, 2013; Bhaskaran *et al.*, 2014).

#### 4. Model set-up

The triangular elements over the model domain (Figure 2a) were created using the Surface water Modelling System software (<https://www.aquaveo.com>). The model domain has approximately  $544 \times 10^3$  triangular elements and  $274 \times 10^3$  nodes. The grid resolution is approximately 500 m near the coastline and 25 km near the open boundary. In the present study, we used the new bathymetry data (Figure 2b) obtained from the study by Krienet *al.* (2016) for conducting model simulations. The dataset incorporated digitised depth values from estuaries and rivers adjoining the head of the BoB. Krienet *al.* (2016) reported improvements in the tidal simulations by using these data. The five major tidal constituents that were used to force a composite tide at the open boundary were  $K_1$  and  $O_1$  (diurnal constituents) and  $M_2$ ,  $S_2$ , and  $N_2$  (semi-diurnal constituents) (Table 1). Amplitudes and phases of these constituents were obtained from the output of Finite Element Solution 2012 (FES2012), a global tidal model (Carrère *et al.*, 2012). A quadratic bottom stress  $\tau_b$  formulation was used in the model and is as follows:

$$\tau_b = \frac{gn^2}{\sqrt[3]{H}} \sqrt{u^2 + v^2}, \quad (1)$$

where  $u$  and  $v$  are depth-averaged velocities,  $g$  is the acceleration due to gravity,  $H = \zeta + h$  is the total water depth,  $\zeta$  is the variation in the water elevation above the mean sea surface,  $h$  is the depth below the mean surface, and  $n$  represents the Manning roughness coefficient. The values of the Manning roughness coefficient were obtained from an earlier study in the region that was conducted by Krienet *al.* (2016). The wetting and drying features were enabled in the model. A time step of 8 s was set to run the model.

**Table 1.** Amplitudes and Greenwich phase lags of tidal constituents forced along the open boundary of the model. A, B, and C represent three open boundary points (Figure 2a).

Constituent		Period (h)	Amplitude (m)			Phase (°)		
Symbol	Name		A	B	C	A	B	C
M <sub>2</sub>	Principal lunar	12.42	0.480	0.475	0.651	076.453	074.301	075.306
S <sub>2</sub>	Principal solar	12.00	0.209	0.206	0.298	104.703	102.734	104.596
N <sub>2</sub>	Larger lunarelliptic	12.66	0.098	0.097	0.133	069.417	064.634	065.057
K <sub>1</sub>	Luni-solar diurnal	23.93	0.118	0.113	0.133	250.375	246.012	238.687
O <sub>1</sub>	Principal lunardiurnal	25.82	0.040	0.038	0.047	240.286	232.709	225.882

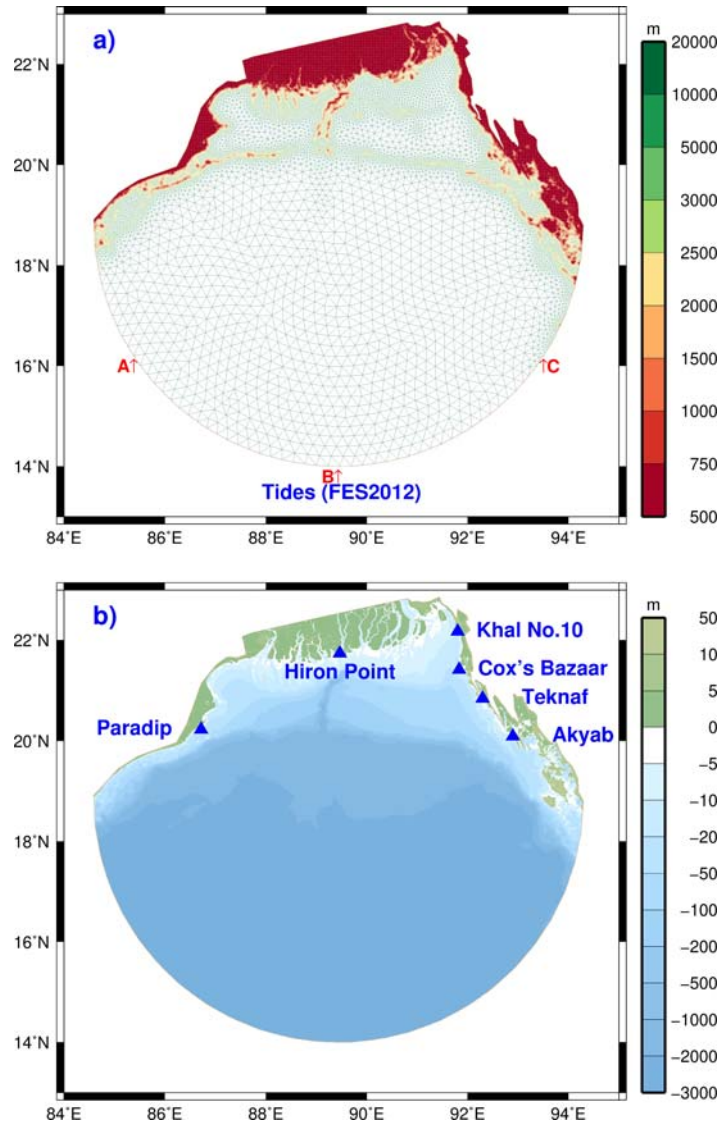


**Figure 2.**(a) Model domain with triangular elements (grid resolution in colour).A, B, and C represent the open boundary points whose tidal amplitudes and phases are presented in Table 1. (b) Topography and bathymetry of the model domain.Triangles were used to mark the stations from which observations were used for validating tides.

## 5. Meteorological forcing

Using parametric models to represent cyclone wind and pressure fields whenever high-resolution meteorological data are not available is a common practice. A parametric cyclone wind-field model developed by Jelesnianski and Taylor (1973) and modified to represent the cyclones in the BoB (Murty *et al.*, 2016) in a better manner was used to construct wind fields of Cyclone Aila. The pressure fields of the cyclone were constructed using the Holland model (Holland, 1980). The model developed by Jelesnianski and Taylor (1973) has been widely used for generating cyclone wind

fields over the BoB. The improved model (Equation 3) considers the strong winds at the outer core region of the cyclones (Murty *et al.*, 2016). The input data used for the parametric models were cyclone core pressure  $P_c$ , maximum wind speed  $V_{max}$ , radius of the maximum wind speed  $R_{max}$ , and the latitude and longitude positions of the cyclone. All these data, except  $R_{max}$ , were obtained from the JTWC best-track archive at a six-hour interval.  $R_{max}$  was calculated using the equation given by Knaff and Zher (2007):

$$R_{max} = 66.785 - 0.09102 V_{max} + 1.0619 (\varphi - 25), \quad (2)$$

where  $\varphi$  is the latitude of the cyclone centre in degrees.

The circular wind field of the cyclone was constructed using the following formula (Murty *et al.*, 2016):

$$W = V_{max} \left( \frac{2rR_{max}}{r^2 + R_{max}^2} \right)^{3/5}, \quad (3) \quad \text{where } r \text{ is}$$

the distance from the centre of the cyclone to any point.

The forward motion of the cyclone was included using the following equation (Jelesnianski, 1966):

$$W_f = V_f \left( \frac{rR_{max}}{r^2 + R_{max}^2} \right), \quad (4) \quad \text{where } V_f \text{ is}$$

the translation velocity of the cyclone.

Wind inflow angle ( $\beta$ ) corrections were applied to the wind field by referring to the study by Harper *et al.* (2001):

$$\beta = \begin{cases} 10 \left( \frac{r}{R_{max}} \right), & 0 \leq r < R_{max}, \\ 10 + 75 \left( \frac{r}{R_{max}} - 1 \right), & R_{max} \leq r < 1.2 R_{max}, \\ 25, & r > 1.2 R_{max}, \end{cases} \quad (5) \quad \begin{array}{l} \text{The} \\ \text{press} \\ \text{ure at} \\ \text{a} \end{array}$$

point was calculated using the Holland model (Holland, 1980) as follows:

$$P = P_c + (P_{env} - P_c) \exp \left[ - \left( \frac{R_{max}}{r} \right)^B \right], \quad (6) \quad \text{where } P_{env} \text{ is}$$

the environmental pressure and that was set to 1013 hPa.

The parameter  $B$  is defined as follows:



$$B = \frac{\rho e V_{max}^2}{P_{env} - P_c}, \quad (7) \quad \text{where}$$

$\rho$  repr

resents the air density and  $e$  is Euler's number.

The wind and pressure fields of Cyclone Aila generated using the parametric models at 06:00 UTC on 25 May 2009 are displayed in Figure 3a and 3b, respectively. In addition to the meteorological fields obtained from the parametric models, we also used 10-m wind and mean sea-level pressure fields obtained from European Centre for Medium-Range Weather Forecast Reanalysis 5 (ECMWF; ERA5) at every  $0.25^\circ$  grid provided every 1 h.

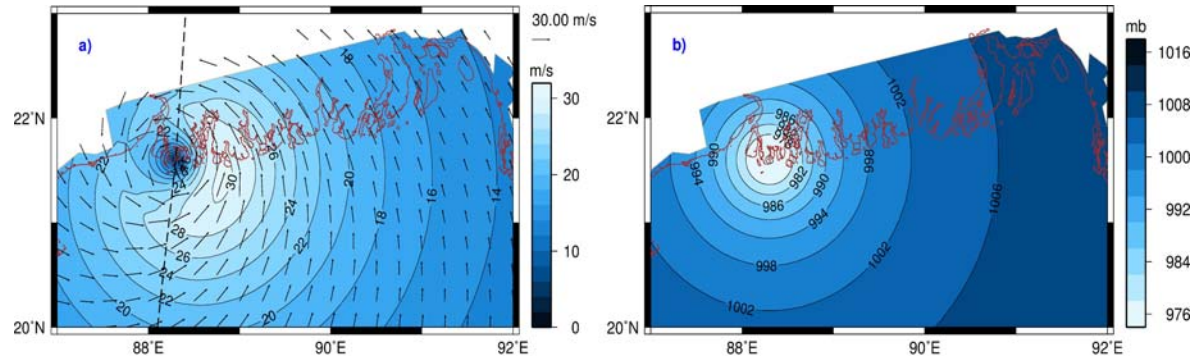


**Figure 3.** (a) Wind and (b) pressure fields at 06:00 UTC on 25 May 2009 constructed using parametric wind and pressure models. The dashed line indicates the track of Cyclone Aila.

## 6. Model simulations

The tide–surge interaction height  $\zeta_I$  can be given as follows:

$$\zeta_I = \zeta_{T+S+I} - (\zeta_S + \zeta_T), \quad (8)$$

which is the difference between water-level height in a coupled tide–surge ( $\zeta_{T+S+I}$ ) simulation and height as a sum of tide ( $\zeta_T$ ) and pure surge ( $\zeta_S$ ) simulations (Banks, 1974). A practical surge  $\zeta_{S+I}$  is defined as the surge including the interaction height (Zhanget al., 2010; Idieret al., 2012):

$$\zeta_{S+I} = \zeta_S + \zeta_I. \quad (9)$$

We conducted the following simulations to obtain the water-level heights on the right-hand side of Equations 8 and 9:

- (i) Forced with tide ( $\zeta_T$ )
- (ii) Forced with wind and pressure ( $\zeta_S$ )
- (iii) Forced with tide, wind, and pressure ( $\zeta_{T+S+I}$ )

Water-level heights from these simulations were used to compute the interaction height and practical surge.

To explore the influence of tides on the tide–surge interaction, experiments were conducted by allowing the cyclone to landfall at different phases of the tidal cycle by shifting its land fall time.

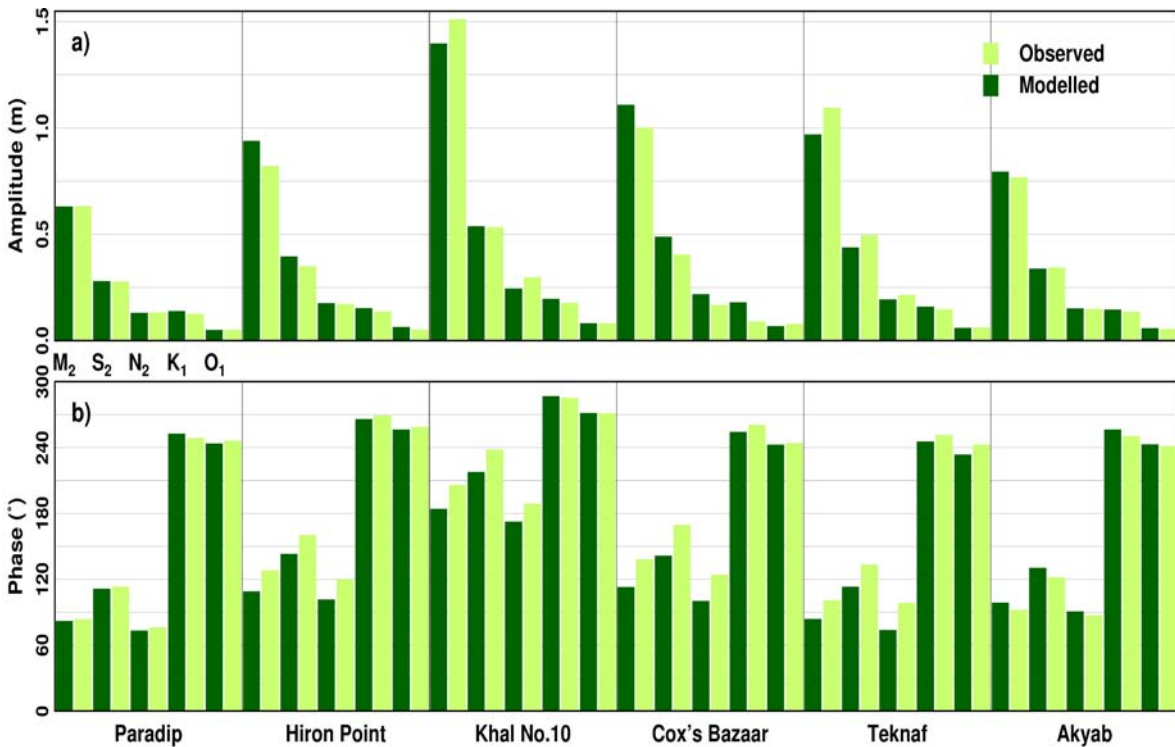


**Figure 4.** Amplitudes and phases of the tidal constituents computed from the model simulations and observations at locations displayed in Figure 2b.

**Table 2.**Error statistics representing the performance of the tide model.

Constituent	Amplitude(m)		Phase(°)	
	MAE	RMSE	MAE	RMSE
M <sub>2</sub>	0.082	0.096	15.184	17.297
S <sub>2</sub>	0.033	0.046	16.131	18.243
N <sub>2</sub>	0.023	0.032	14.843	17.240
K <sub>1</sub>	0.027	0.039	4.424	4.744
O <sub>1</sub>	0.005	0.007	2.852	3.986
Average	0.034	0.044	10.687	12.302

## 7. Validation of simulated tides

For validating the simulated tides, we used tidal constituents obtained by conducting a harmonic analysis on the sea-level data from six tide gauges (Figure 2b) spanning across a full year. The sea-level data were provided by the Survey of India (SOI), the Indian National Centre for Ocean Information Services (INCOIS), and the Sea Level Center, University of Hawaii. Sixty-three tidal constituents were used in the harmonic analysis by using the Tidal Analysis Software Kit 2000 (TASK-2000; Bell *et al.*, 1999). The agreement between the tidal constituents computed from the modelled and observed time series was quantified by calculating the mean absolute error (MAE) and root mean square error (RMSE) as follows:

$$MAE = \frac{1}{N} \sum_{i=1}^N |(Y_m)_i - (Y_o)_i|, \quad (10)$$

$$RMSE = \sqrt{\frac{1}{N} \sum_{i=1}^N [(Y_m)_i - (Y_o)_i]^2}, \quad (11)$$

where  $N$  represents the total number of constituents,  $Y_m$  presents the modelled constituents, and  $Y_o$  is the observed constituent. The error statistics are presented in Table 2 for five tidal constituents. For providing a visual comparison, the amplitudes and phases of these constituents from the model and observations are presented in Figure 4. Overall, the model reproduced amplitudes and phases of the tidal constituents reasonably well. The average MAEs were approximately 0.034 m and  $10.687^\circ$  and average RMSEs were approximately 0.044 m and  $12.302^\circ$  for the amplitudes and phases of the tidal constituents, respectively.

### 8. Storm surge

The time series of model-simulated practical surges and water level at Hiron Point are displayed in Figure 5 along with observations from the tide gauge. Two model simulations are displayed in the figure—one forced with meteorological fields from the parametric models (based on the JTWC data) and the other one forced with the ERA5 data. The error statistics of the performance of the model are presented in Table 3. The time series of the observed surge was obtained by de-tiding the hourly sea-level data of 2009. The sea-level data were provided by the Bangladesh Inland Water Transport Authority (BIWTA). Sixty-three tidal constituents including annual  $S_a$  and semi-annual  $S_{sa}$  constituents were used in the de-tiding process by using TASK-2000. The tide gauge at Hiron Point, which is located approximately 130 km from the cyclone landfall location, recorded a storm surge of approximately 1.73 m. The corresponding JTWC and ERA5 surges were approximately 1.23 and 1.35 m, respectively (Figure 5a). The observed surge time series revealed a gradual development of the storm surge. The surge event exhibited two peaks that differed by approximately 0.5 m in height and 8 h in time. The observed surge was much longer (remained above 1 m for approximately 15 h) than the simulated surge. The aforementioned features of the storm surge were missing in the JTWC simulation, whereas the ERA5 simulation reproduced variations in the surge curve but with an underestimation. The error statistics (Table 3) indicate that the ERA5 data simulation was better than the JTWC data simulation, with a decrease in the RMSE from 0.42 to 0.24 m and a small increase in the correlation from 0.86 to 0.90. Although time series comparison at Hiron Point revealed that the ERA5 surge data exhibited better results than the JTWC surge data, the JTWC surge data exhibited better results for the maximum surge near the landfall location than the ERA5 surge data. There was an underestimation in the surge heights by approximately 30%–50% near the

landfall location in the ERA5 data simulation compared with the surge heights of the JTWC data simulation (Figure 6). Nevertheless, the ERA5 data simulation indicates that errors in the atmospheric input can be the major cause for the discrepancies in the JTWC simulated surge at Hiron Point. The observed total water level after eliminating the mean was approximately 2.63 m (Figure 5b) and the simulated water levels were approximately 2.28 and 2.43 m for the JTWC and ERA5 simulations, respectively. As in the case of a storm surge, the ERA5 simulation performed better than the JTWC simulation in terms of the water level (Table 3).

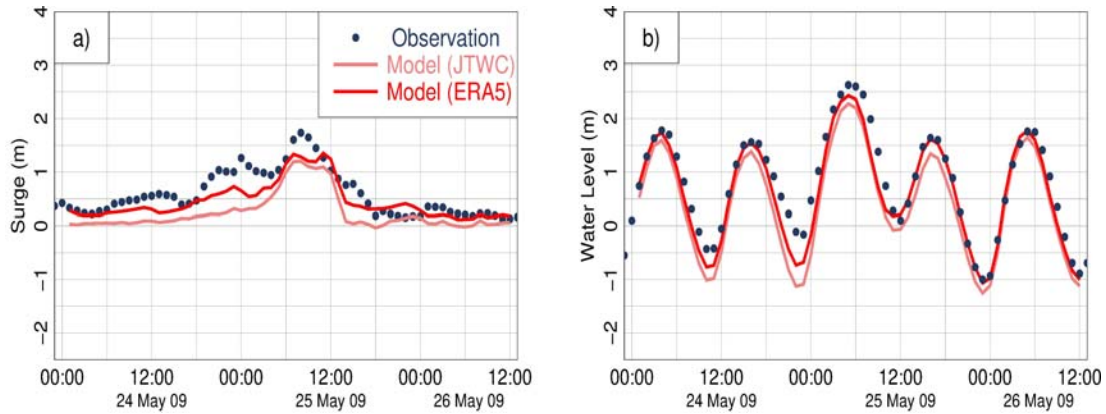


**Figure 5.** Time series of the observed (circle) and modelled (continuous line) (a) storm surges and (b) water levels at Hiron Point during Cyclone Aila. The modelled surge is the practical surge (including tide–surge interaction). The observed water level is shown after eliminating the mean over a period of one year.

**Table 3.** Error statistics representing the performance of the coupled tide–surge model.

Location	JTWC				ERA5			
	Water level		Surge		Water level		Surge	
	RMSE(m)	r	RMSE(m)	r	RMSE(m)	r	RMSE(m)	r
Hiron Point	0.47	0.97	0.42	0.86	0.28	0.98	0.24	0.90

The spatial distribution of the maximum practical surge (Figure 6a) simulated using the JTWC data revealed that the surge during Cyclone Aila reached above 3 m inside the estuarine

channels at the right side of the cyclone landfall location. The surge heights reached above 1 m along the shallow coastal waters and thus extended to the regions that were within approximately 200 km at the right side of the landfall location. Moreover, the surge reached some regions to the northeast of the head of the BoB that are almost 350 km away from the landfall location. The ERA5 simulation (Figure 6b) revealed a similar surge pattern over the coastal waters but failed to reproduce the maximum surge near the cyclone landfall location. Overall, the performance of the JTWC simulation was satisfactory because it could reproduce the reported maximum surge height (approximately 3 m) during the event.

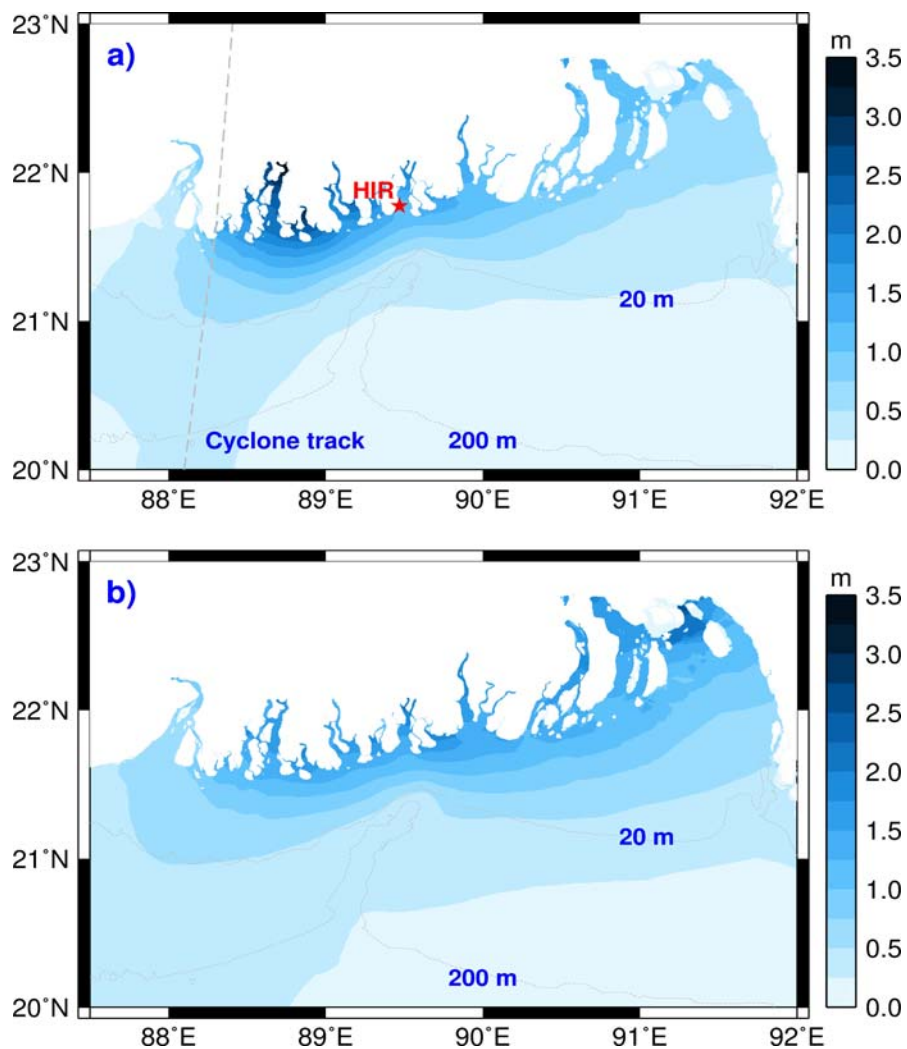


**Figure 6.** Maximum practical surge during Cyclone Aila obtained from the (a) JTWC and (b) ERA5 simulations. The location of the Hiron Point (HIR) tide gauge is marked using a star. The depth contours of 20 and 200 m are also shown.

## 9. Tide–surge interaction

The time series of various water-level heights (Equations 8 and 9) during Cyclone Aila at four locations (Figure 9a) are displayed in Figure 7. Location L1 lies within the region in which the maximum open coast surge was observed in the JTWC simulation. Locations L2 and L3 lie in the northeastern part of the head of the BoB. At L1 and Hiron Point, the interaction curves exhibited nearly similar patterns with a positive interaction during low tide and negative interaction during high tide (Figure 7a and b). This interaction pattern indicates that the surge height decreased during high tides and increased during low tides. The JTWC and ERA5 interaction patterns at L1 and Hiron Point were almost consistent. The interaction patterns of the two model simulations were inconsistent at the locations considered in the northeastern part (L2 and L3) due to the differences between the pure surges. The magnitudes of the pure surges in the JTWC and ERA5 simulations are nearly the same at L2 and L3 (approximately 1 m). However, the ERA5 pure surge was longer in terms of the duration than the JTWC pure surge. Moreover, the JTWC pure surge had negative heights, whereas the ERA5 pure surge was positive throughout. The practical surge increased due to the interaction and decreased for the ERA5 and JTWC simulations in comparison to their pure surges. Another interesting feature to note at L2 and L3 is how the difference in the surge curves between the two simulations influenced the total water levels. The JTWC water levels exceeded the peak predicted tide only once, whereas the ERA5 water levels exceeded the peak predicted tide twice. The obtained time series reveals that at all the locations, the maximum water level obtained from the coupled tide–surge model was lower than that obtained using the linear sum of the tide and surge (uncoupled). Thus, the tide–surge interaction decreased the maximum water levels.

The tide–surge interaction characteristics (based on the JTWC simulations) of three locations in the estuarine channel in which the maximum surge occurred are depicted in Figure 8. Over a distance of approximately 40 km from the mouth of the channel (L4) to the inner location of the channel (L6), the practical surge increased from 2 to 3 m. The interaction curves were similar at L4 and L6 but with different magnitudes. The interaction was high at low and high tides, and the maximum values attained a height of approximately 0.5 m at L4 and approximately 1 m at L6. The interaction caused the practical surge at the inner location to be lower in magnitude and to delay by approximately 1.5 h compared with the pure surge. The estimated maximum water levels provided by the uncoupled model were higher than approximately 0.3, 0.45, and 0.7 m at L4, L5, and L6, respectively, compared with those obtained from the coupled model.



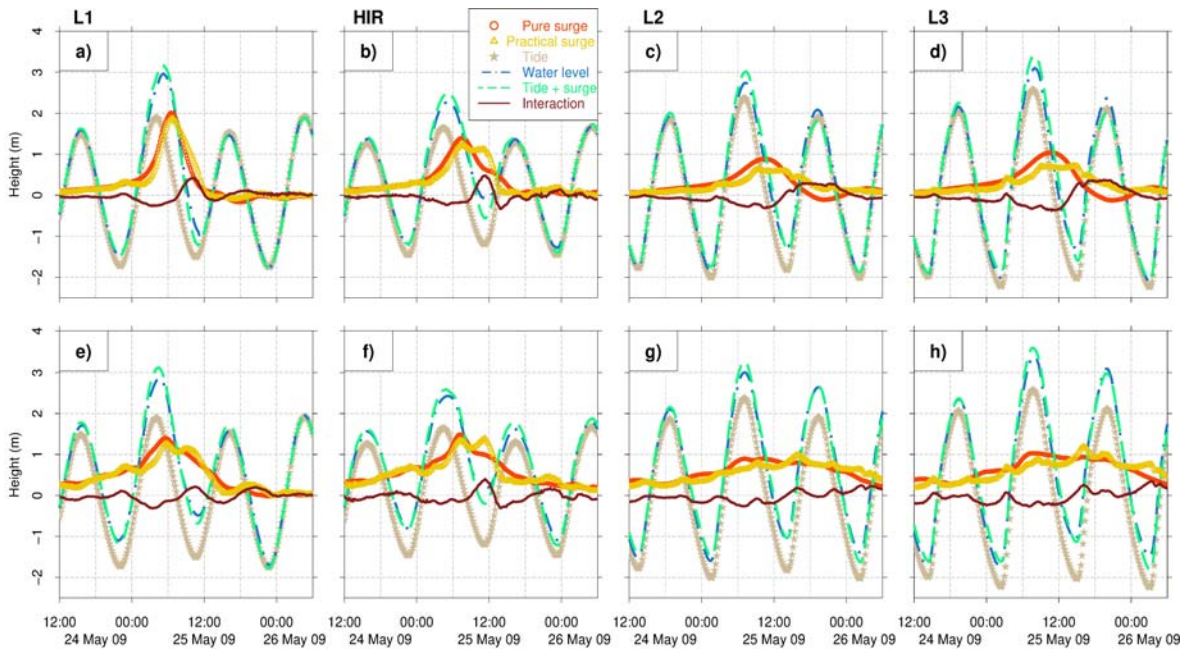


**Figure 7.** Time series of various water level heights during Cyclone Aila at the locations displayed in Figure 9a. The upper panels (a–d) present the results from the JTWC simulations and the lower panels (e–h) present the results from the ERA5 simulations. The height obtained from the coupled tide–surge model is indicated as ‘Water level’, and the height obtained using the sum of tide and surge (uncoupled) is indicated as ‘Tide + surge’.

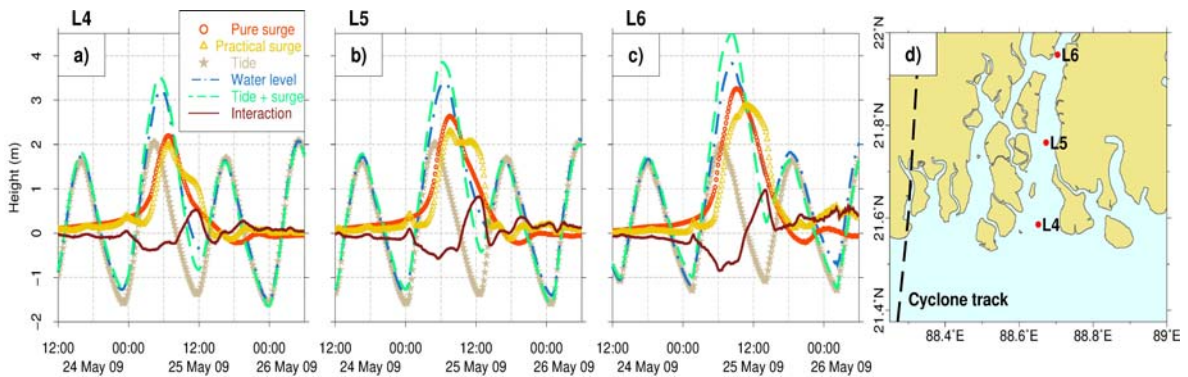


**Figure 8.** (a–c) Time series of various water level heights based on the JTWC simulations at locations in the estuarine channel where the maximum surge occurred. (d) Map of the locations.



The spatial pattern of the maximum absolute values of the interaction heights (maximum $|\zeta_I|$ ) during Cyclone Ailais illustrated in Figure 9. Tide–surge interaction was significant in the shallow waters of the head of the BoB and exhibited values greater than 0.1 m that were confined within the 20-m isobaths. The results from the JTWC simulation (Figure 9a) indicated that interaction was high near the maximum surge region, the northeastern part of the head of the BoB, and inside the estuarine channels and attained magnitudes of up to 1 m. The spatial pattern of the interaction exhibited lower values in the central region of the head of the BoB and higher values on either sides (eastern and western sides) of this minimum. The ERA5 simulation indicated a similar spatial pattern but failed to reproduce the strong interaction on the right side of the cyclone landfall location (Figure 9b). Positive differences were observed between the maximum water levels in the uncoupled and coupled JTWC simulations (Figure 10). This finding indicates that the maximum water levels decreased in the domain due to the tide–surge interaction. The differences were up to 0.3 m in the open coastal waters and upto 1 m inside the estuarine channels.

Because storm surges are influenced by tide–surge interaction, ‘skew surge’ is a useful measure to quantify the genuine contribution of meteorological forces (de Vries *et al.*, 1995; Williams *et al.*, 2016). Skew surge is defined as the difference between the peak water level and the nearest (in time) predicted high tide. Therefore, by definition, a skew surge quantifies the additional water level above the predicted high tide. Figure 11 illustrates the skew surge during Cyclone Aila that was obtained from the JTWC simulations. The maximum skew surge was approximately 2 m, and most of the coastal regions in the head of the BoB experienced water levels of 0.5 m or more above the predicted high tide.

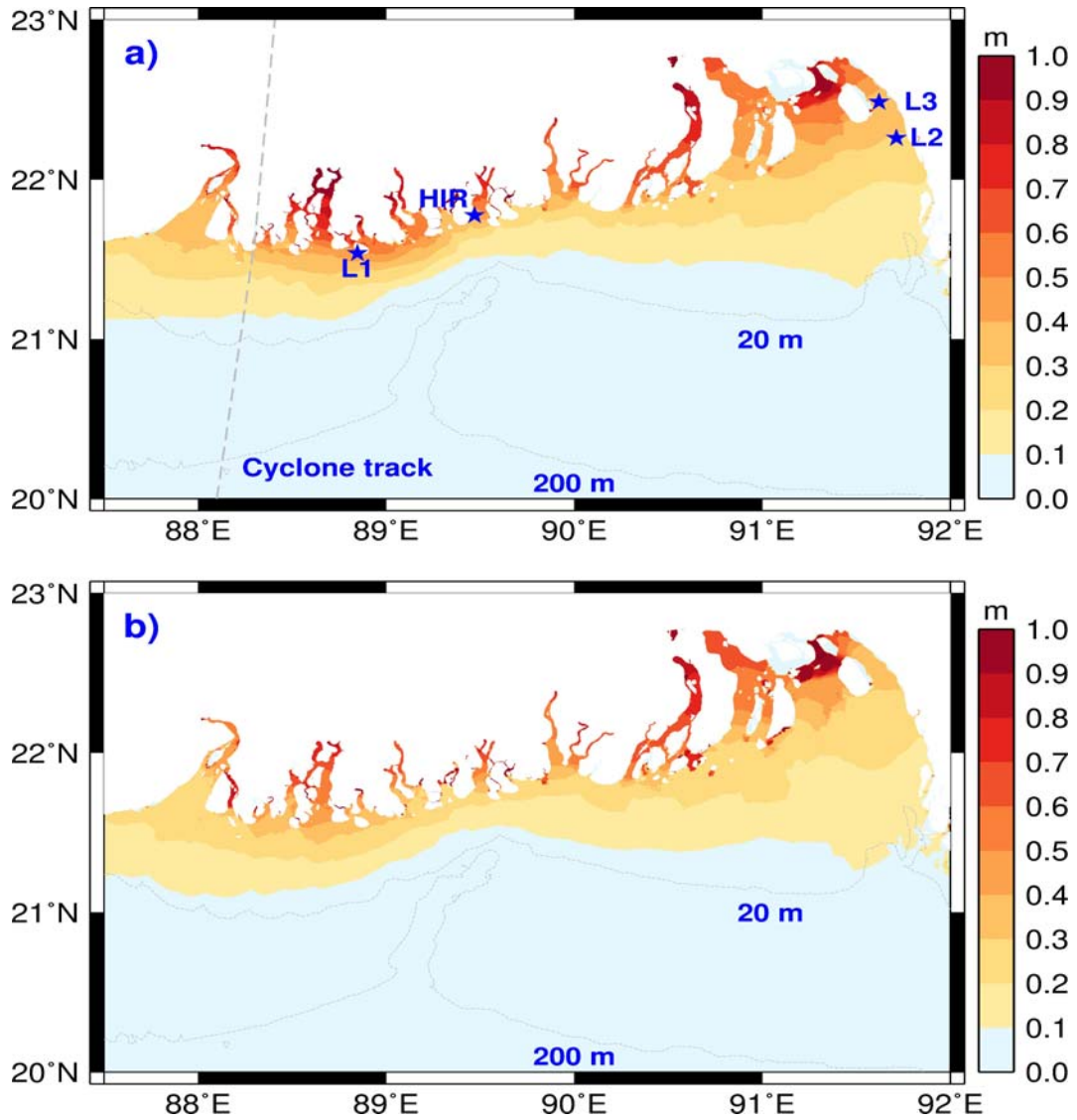


**Figure 9.** Spatial distribution of the maximum absolute interaction heights(maximum  $|\zeta_I|$ ) in the (a) JTWC and (b) ERA5 simulations. The locations for the related time series are presented in Figure 7 and marked with stars. Moreover, the 20- and 200-m isobaths are depicted.

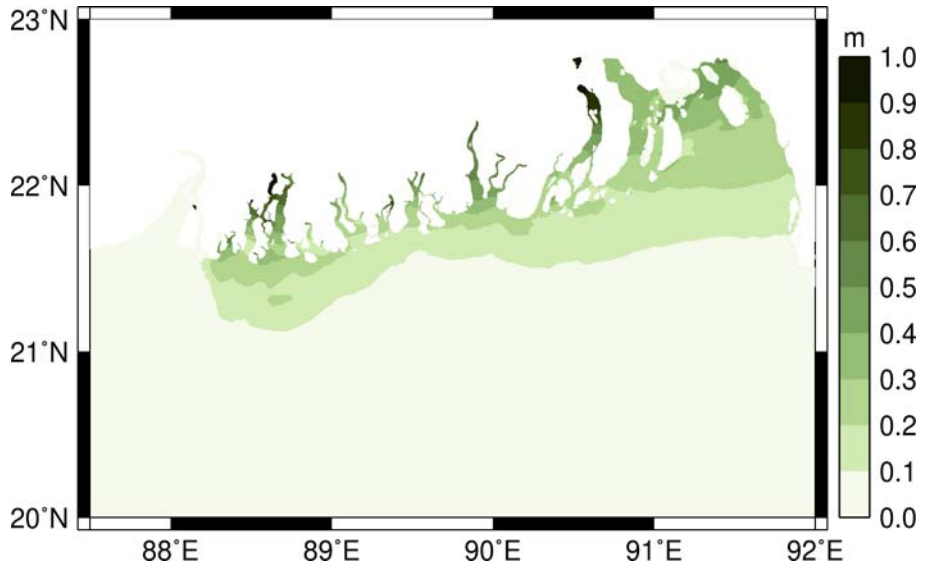


**Figure 10.** Spatial distribution of the differences between the maximum water levels (uncoupled minus coupled) during Cyclone Aila obtained from the JTWC simulations.

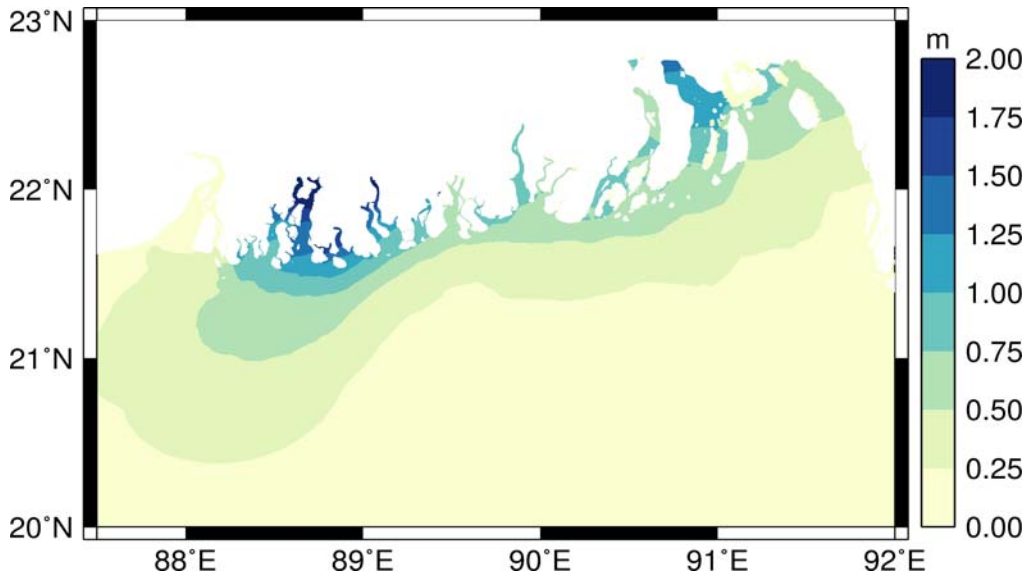


**Figure 11.** Spatial distribution of the skew surge heights during Cyclone Aila based on the JTWC simulations.

## 10. Influence of tidal phases

The time series of practical surges (JTWC simulations) of Cyclone Aila for landfalls at various phases of the tide at L1 (Figure 13a) are presented in Figure 12. The figure indicates how the practical surge and maximum water level would have varied if Cyclone Aila had occurred at different phases of the tidal cycle. For the given pure surge, the computed practical surge had higher surge heights during low tides and lower surge heights during high tides. The practical surges close to the high tide were smaller than their pure surge counter parts, and those close to the low tide were higher than their pure surge counter parts. For the coupled simulations, more than 1 m change occurred between maximum water levels for cyclone landfalls at low and high tides at L1.

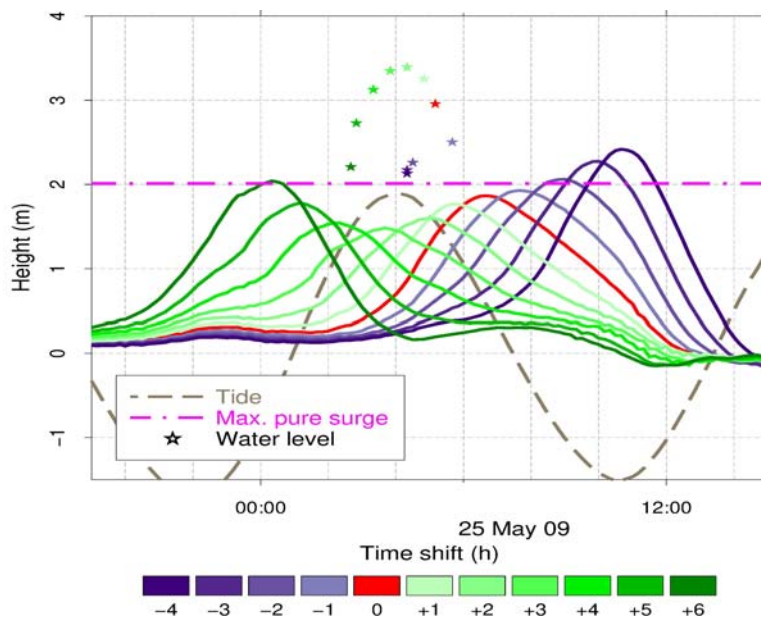


**Figure 12.** Practical surges (continuous lines) at L1 for various time-shifted landfalls of Cyclone Aila. A positive (negative) time shift indicates the surge leading (lagging) the original surge simulation (red curve). Stars indicate maximum water levels from the coupled models. The simulations are based on the JTWC data.

Spatial maps of the possible maximum water levels due to the different phases of a tidal cycle are useful for flood risk analysis and management purposes. The illustrations presented in Figure 13 show the percentage of change in the maximum water levels (JTWC simulations) due to the cyclone landfalls at high and low tides with respect to that of the original Cyclone Aila. Water levels would have been up to 20% higher in the case of a cyclone landfall during a high tide and would have been approximately 40% lower in the case of a landfall during a low tide compared with the

original water levels. The results indicate the substantial influence of the tidal cycle on the maximum water levels.

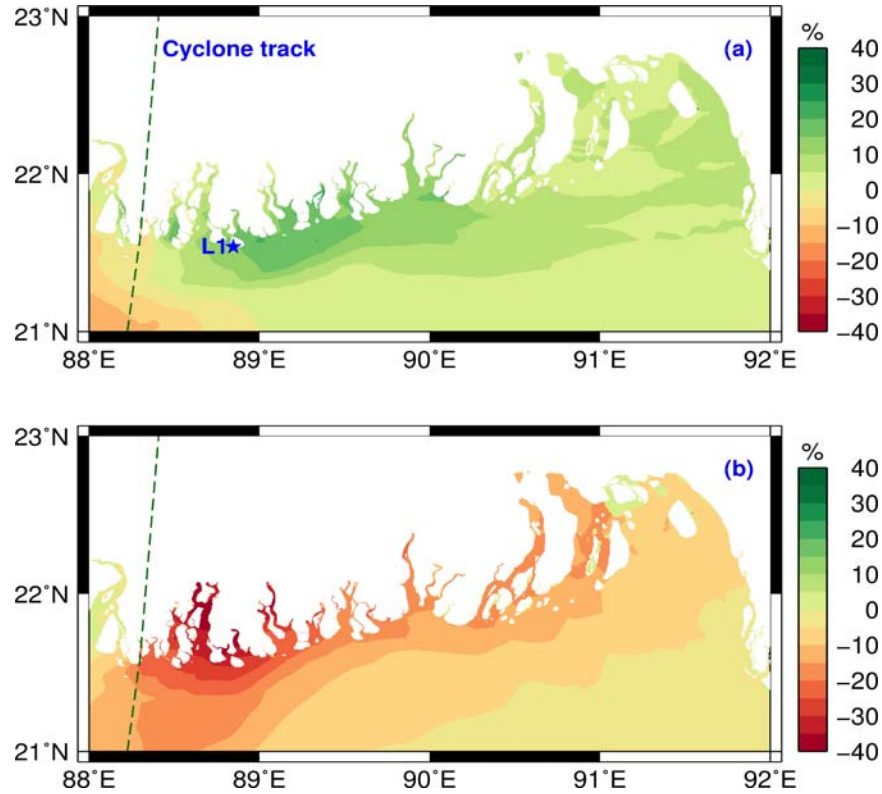


**Figure 13.** Spatial distribution of the changes in the maximum water levels (in percentage) with respect to the original Cyclone Aila water levels (a) for a high-tide landfall of Cyclone Aila and (b) for a low-tide landfall of Cyclone Aila. The simulations are based on the JTWC data.

## 11. Discussion

An investigation using numerical modelling was conducted to study the tide–surge interaction at the head of the BoB during Cyclone Aila. A significant amount of interaction was found during the event and reached up to 1 m in the estuarine channels, near the region where the surge value was maximum, and in the northeastern part of the head of the BoB. The interaction was negligible in deep waters (depths greater than 20m). Although the interaction curve had both negative and positive heights, the overall effect of the tide–surge interaction was the reduction in the maximum water levels.

The extensive area covering the northeastern part of the head of the BoB is shallow and has depths lower than approximately 10 m (Krienet *al.*, 2017). The tide–surge interaction can be

significant when both tide and surge interact while propagating over a large distance towards the coast (Rossiter, 1961). Moreover, the presence of islands in the northeastern part may enhance tides, surges, and their interaction through a channelling effect that was proposed by Zhang *et al.* (2010) for a Taiwan Strait case. A high amount of interaction was noticed in this region during Cyclone Aila. In addition to the northeastern part of the head of the BoB, regions in and around the maximum surge had a high tide–surge interaction during the event. This phenomenon is similar to the conclusion given by Rego and Li (2010), who observed a significant interaction near the highest surge while studying Hurricane Rita in the Gulf of Mexico. The spatial distribution of the maximum interaction during Cyclone Aila revealed that the tide–surge interaction was relatively small in the central part of the head of the BoB. In a recent study on storm surge processes along the west coast of India, Poulouse *et al.* (2018) revealed that the interaction strengthens with increase in the continental shelf width and tidal amplitude. The central part of the head of the BoB is characterised by relatively lower tidal amplitudes (Sindhu and Unnikrishnan, 2013) and reduced width of the continental shelf (due to the presence of a large submarine canyon). These features can probably explain the relatively reduced tide–surge interaction at the central part of the domain.

The variation in the tidal amplitude over the tidal cycle indicates significant influence on the storm surge and total water level. The surges that were generated when the cyclone landfall occurred during a low tide were larger than those generated when the cyclone landfall occurred during a high tide. The surge height variability with respect to the tidal condition can be related to the effect of the total water depth change due to different phases of the tide. According to Horsburgh and Wilson (2007), the water-level elevation due to wind stress is inversely proportional to the total water depth ( $\zeta \propto \tau_s / gH$ , where  $\zeta$  is the water-level elevation and  $\tau_s$  is the wind stress). This relationship indicates that the surge height is larger at a low tide compared with that at a high tide under the same meteorological conditions.

The storm surge simulated using the JTWC data failed to capture the variation in the observed data. Because the ERA5 data simulation captured the surge variations to a certain extent, the data indicated that the discrepancy in the JTWC surge can be largely due to errors in the meteorological fields. Capturing the full variation in the surge curve is crucial for accurately predicting coastal flooding (Lyddon *et al.*, 2018). The long-duration surge observed at Hiron Point resulted in multiple peaks. The generation of multiple peaks in the case of a long-duration surge (lasting more than a tidal cycle) due to tide–surge interaction was recognised previously (Horsburgh and Wilson, 2007). Locations in the northeastern part were significantly influenced by such a long duration event, as indicated by the ERA5 simulations. The water levels from the ERA5 simulation

exceeded the peak predicted tides twice in comparison to that from the JTWC simulation in the northeastern part. Therefore, capturing the full surge curve, along with the maximum surge, is crucial for accurately predicting the water level.

## **12. Conclusions**

The Tide–surge interaction phenomenon has crucial practical applications because of its role in modifying the total water level. Thus, this interaction is a key component for conducting reliable water level predictions. Although the present study is specific to Cyclone Aila, it revealed that the total water levels are significantly influenced by tide–surge interaction process even during relatively low-intensity cyclones (for example, Category 1 cyclones). The tide–surge interaction and total water level are sensitive to the time profiles of a surge curve. This indicates that the variability in the surge should be reproduced accurately to reduce the uncertainties in flood hazard predictions. Tide–surge interaction is remarkable at the head of the BoB, which should be considered in numerical modelling simulations. Even a few tens of centimetres of change in the water level can have a significant influence on flooding in the low-lying coastal areas of this region.

## **Acknowledgements**

The first author thanks the University Grants Commission (UGC) for providing the research fellowship. We thank the SOI, INCOIS, and BIWTA for providing the tide-gauge data. The first author acknowledges the useful discussions with Fabien Durand and Laurent Testut. Numerical computations were conducted using the HPC facility (Pravah) at CSIR-NIO. Thanks to ADCIRC developers for making the model code freely available. Graphs and maps were generated using Generic Mapping Tools (Wessel and Smith, 2013) and Figure Gen (Dietrich *et al.*, 2013). This study is CSIR-NIO contribution No.XXX.

## References

- Antony C Unnikrishnan AS (2013) Observed characteristics of tide-surge interaction along the east coast of India and the head of Bay of Bengal. *Estuarine, Coastal and Shelf Science* 131, pp.6-11. <https://doi.org/10.1016/j.ecss.2013.08.004>
- As-Salek JA Yasuda T (2001) Tide-surge interaction in the Meghna estuary: most severe conditions. *Journal of Physical Oceanography* 31, pp.3059-3072. [https://doi.org/10.1175/1520-0485\(2001\)031<3059:TSIITM>2.0.CO;2](https://doi.org/10.1175/1520-0485(2001)031<3059:TSIITM>2.0.CO;2)
- Banks JE (1974) A mathematical model of a river-shallow sea system used to investigate tide, surge and their interaction in the Thames-Southern North Sea region. *Philosophical Transactions of the Royal Society of London A: Mathematical, Physical and Engineering Sciences* 275(1255), pp.567-609. <https://doi.org/10.1098/rsta.1974.0002>
- Bell C Vassie JM Woodworth PL (1999). POL/PSMSL Tidal Analysis Software Kit 2000 (TASK-2000), Permanent Service for Mean Sea Level, CCMS Proudman Oceanographic Laboratory, Bidston Observatory, Birkenhead, Merseyside CH43 7RA, U.K.
- Bhaskaran PK Gayathri R Murty PLN Bonthu S Sen D (2014) A numerical study of coastal inundation and its validation for Thane cyclone in the Bay of Bengal. *Coastal Engineering* 83, pp.108-118. <https://doi.org/10.1016/j.coastaleng.2013.10.005>
- Carrère, L Lyar F Cancet M GuillotARoblou L (2012) FES2012: A new global tidal model taking advantage of nearly 20 years of altimetry. Paper presented at The Symposium 20 Years of Progress in Radar Altimetry, Venice, Italy.
- Das PK Sinha MC Balasubramanyam V (1974) Storm surges in the Bay of Bengal. *Quarterly Journal of the Royal Meteorological Society* 100(425), pp.437-449. <https://doi.org/10.1002/qj.49710042515>
- Dawson C Westerink JJ Feyen JC Pothina D (2006): Continuous, discontinuous and coupled discontinuous-continuous Galerkin finite element methods for the shallow water equations. *International Journal for Numerical Methods Fluids*, 52(1), pp.63-88. <https://doi.org/10.1002/fld.1156>
- deVries H Breton M de Mulder T Krestenitis Y Proctor R Ruddick K Salomon JC Voorrips A (1995) A comparison of 2D storm surge models applied to three shallow European seas. *Environmental Software*, 10(1), pp.23-42. [https://doi.org/10.1016/0266-9838\(95\)00003-4](https://doi.org/10.1016/0266-9838(95)00003-4)
- Dietrich JC Dawson CN Proft JM Howard MT Wells G Fleming JG Luettich RA Westerink JJ Cobell Z Vitse M Lander H (2013) Real-time forecasting and visualization of hurricane waves and storm surge using SWAN+ADCIRC and FigureGen. In: Dawson C Gerritsen M (eds) *Computational challenges in the geosciences. The IMA Volumes in Mathematics and its Applications* 156, Springer, New York, pp.49-70. [https://doi.org/10.1007/978-1-4614-7434-0\\_3](https://doi.org/10.1007/978-1-4614-7434-0_3)
- Doodson AT (1929) Report on Thames floods, *Geophysical memoirs*, Lond, 47, pp.1 –26.



- Feng X Olabarrieta M Valle-Levinson A (2016) Storm-induced semidiurnal perturbations to surges on the US Eastern Seaboard. *Continental Shelf Research* 114, pp.54-71. <https://doi.org/10.1016/j.csr.2015.12.006>
- Flierl GR Robinson AR (1972) Deadly surges in the Bay of Bengal: Dynamics and storm-tide tables. *Nature*, 239(5369), pp.213-215. <https://doi.org/10.1038/239213a0>
- Frank NL Husain SA (1971) The deadliest tropical cyclone in history. *Bulletin of the American Meteorological Society* 52(6), pp.438-445. [https://doi.org/10.1175/1520-0477\(1971\)052<0438:TDTCIH>2.0.CO;2](https://doi.org/10.1175/1520-0477(1971)052<0438:TDTCIH>2.0.CO;2)
- Fritz HM Blount CD Thwin S Thu MK Chan N (2009) Cyclone Nargis storm surge in Myanmar. *Nature Geoscience* 2(7), pp.448-449. <https://doi.org/10.1038/ngeo558>
- Gayathri R Murty N Bhaskaran PK Kumar TS (2016) A numerical study of hypothetical storm surge and coastal inundation for AILA cyclone in the Bay of Bengal. *Environmental Fluid Mechanics* 16(2), pp.429-452. <https://doi.org/10.1007/s10652-015-9434-z>
- Harper B Hardy T Mason L Bode L Young I Nielsen P (2001). *Queensland Climate Change and Community Vulnerability to Tropical Cyclones, Ocean Hazards Assessment - Stage 1*. Brisbane, Queensland, Australia: Department of Natural Resources and Mines, p383.
- Holland GJ (1980). An analytic model of the wind and pressure profiles in hurricanes. *Monthly weather review* 108(8), pp.1212-1218. [https://doi.org/10.1175/1520-0493\(1980\)108<1212:AAMOTW>2.0.CO;2](https://doi.org/10.1175/1520-0493(1980)108<1212:AAMOTW>2.0.CO;2)
- Horsburgh KJ Wilson C (2007) Tide-surge interaction and its role in the distribution of surge residuals in the North Sea. *Journal of Geophysical Research* 112, C08003. <https://doi.org/10.1029/2006JC004033>
- Hussain MA Tajima Y (2017) Numerical investigation of surge–tide interactions in the Bay of Bengal along the Bangladesh coast. *Natural Hazards* 86(2), pp.669-694. <https://doi.org/10.1007/s11069-016-2711-4>
- Idier D Dumas F Muller H (2012) Tide-surge interaction in the English Channel. *Natural Hazards and Earth System Sciences* 12(12), p.3709-3718. <https://doi.org/10.5194/nhess-12-3709-2012>
- IFNet (2009) International Flood Network secretariat/ Infrastructure Development Institute-Japan, June 24, 2009. <http://www.internationalfloodnetwork.org/aila.htm>
- Jelesnianski CP Taylor AD (1973) A Preliminary View of Storm Surges before and after Storm Modifications. NOAA Technical Memorandum. ERL WMPO-3, National Oceanic and Atmospheric Administration, U.S. Department of Commerce, p. 33.
- Jelesnianski CP (1966). Numerical computations of storm surges without bottom stress. *Monthly Weather Review*, 94(6), pp.379-394. [https://doi.org/10.1175/1520-0493\(1966\)094<0379:NCOSSW>2.3.CO;2](https://doi.org/10.1175/1520-0493(1966)094<0379:NCOSSW>2.3.CO;2)
- Johns B Ali MA (1980) The numerical modelling of storm surges in the Bay of Bengal. *Quarterly journal of royal meteorological society* 106 (447), pp.1-18. <https://doi.org/10.1002/qj.49710644702>

Knaff JA Zehr RM (2007) Reexamination of tropical cyclone wind–pressure relationships. *Weather and forecasting* 22(1), pp.71-88. <https://doi.org/10.1175/WAF965.1>

Krien Y Mayet C Testut L Durand F Tazkia AR Islam AKMS Gopalakrishna VV Becker M Calmant S Shum CK Khan ZH (2016) Improved bathymetric dataset and tidal model for the northern Bay of Bengal. *Marine Geodesy* 39(6), pp.422-438. <https://doi.org/10.1080/01490419.2016.1227405>

Krien Y Testut L Islam AKMS Bertin X Durand F Mayet C Tazkia AR Becker M Calmant S Papa F Ballu V (2017) Towards improved storm surge models in the northern Bay of Bengal. *Continental Shelf Research* 135, pp.58-73. <https://doi.org/10.1016/j.csr.2017.01.014>

Luettich Jr RA Westerink JJ Scheffner NW (1992) ADCIRC: An Advanced Three-Dimensional Circulation Model for Shelves, Coasts, and Estuaries. Report 1.Theory and Methodology of ADCIRC-2DDI and ADCIRC-3DL (No.CERC-TR-DRP-92-6).COASTAL ENGINEERING RESEARCH CENTER VICKSBURG MS.

Luettich RA and Westerink JJ (2004): Formulation and numerical implementation of the 2D/3D ADCIRC finite element model version 44.XX. 74 pp. [Available online at [https://adcirc.org/files/2018/11/adcirc\\_theory\\_2004\\_12\\_08.pdf](https://adcirc.org/files/2018/11/adcirc_theory_2004_12_08.pdf)].

Lyddon C Brown JM Leonardi N Plater AJ (2018) Uncertainty in estuarine extreme water level predictions due to surge-tide interaction. *PloS one*, 13(10), e0206200. <https://doi.org/10.1371/journal.pone.0206200>

Murty PLN Bhaskaran PK Gayathri R Sahoo B Kumar TS SubbaReddy B (2016) Numerical study of coastal hydrodynamics using a coupled model for Hudhud cyclone in the Bay of Bengal. *Estuarine, Coastal and Shelf Science* 183, pp.13-27. <https://doi.org/10.1016/j.ecss.2016.10.013>

Needham H Keim BD Sathiaraj D (2015) A Review of Tropical Cyclone-Generated Storm Surges: Global Data Sources, Observations and Impacts. *Reviews of Geophysics* 53(2), pp.545-591. <https://doi.org/10.1002/2014RG000477>

Park YH Suh KD (2012) Variations of storm surge caused by shallow water depths and extreme tidal ranges. *Ocean Engineering* 55, pp.44-51. <https://doi.org/10.1016/j.oceaneng.2012.07.032>

Paul GC Ismail AIM Rahman A Karim MFHoque A (2016) Development of Tide–Surge Interaction Model for the Coastal Region of Bangladesh. *Estuaries and coasts* 39(6), pp.1582-1599. <https://doi.org/10.1007/s12237-016-0110-4>

Poulose J Rao AD Bhaskaran PK (2018). Role of continental shelf on non-linear interaction of storm surges, tides and wind waves: An idealized study representing the west coast of India. *Estuarine, Coastal and Shelf Science*, 207, pp.457-470.<https://doi.org/10.1016/j.ecss.2017.06.007>

Prandle D Wolf J (1978) The interaction of surge and tide in the North Sea and River Thames. *Geophysical Journal of the Royal Astronomical Society* 55(1), pp.203-216. <https://doi.org/10.1111/j.1365-246X.1978.tb04758.x>

Proudman J (1955) The propagation of tide and surge in an estuary. In *Proceedings of the Royal Society of London A: Mathematical, Physical and Engineering Sciences* 231(1184), pp. 8-24. <https://doi.org/10.1098/rspa.1955.0153>

Rao AD Murty PLN Jain I Kankara RS Dube SK Murty TS (2013) Simulation of water levels and extent of coastal inundation due to a cyclonic storm along the east coast of India. *Natural hazards* 66(3), pp.1431-1441. <https://doi.org/10.1007/s11069-012-0193-6>

Rego JL Li C (2010) Nonlinear terms in storm surge predictions: Effect of tide and shelf geometry with case study from Hurricane Rita. *Journal of Geophysical Research: Oceans* 115(C6). <https://doi.org/10.1029/2009JC005285>

Rose L Bhaskaran PK (2017) Tidal propagation and its non-linear characteristics in the Head Bay of Bengal. *Estuarine, Coastal and Shelf Science*, 188, pp.181-198. <https://doi.org/10.1016/j.ecss.2017.02.024>.

Rossiter JR (1961) Interaction between tide and surge in the Thames. *Geophysical Journal International* 6(1), pp.29-53. <https://doi.org/10.1111/j.1365-246X.1961.tb02960.x>

Roy K Kumar U Mehedi H Sultana T Ershad D M (2009) Initial Damage Assessment Report of Cyclone AILA with focus on Khulna District. UnnayanOnneshan-Humanity Watch- Nijera Kori, Khulna, Bangladesh, June 23, 2009. pp.31. [https://www.researchgate.net/publication/273771123\\_Cyclone\\_Aila\\_2009\\_Initial\\_Assessment\\_Report\\_with\\_focus\\_on\\_Khulna\\_District](https://www.researchgate.net/publication/273771123_Cyclone_Aila_2009_Initial_Assessment_Report_with_focus_on_Khulna_District) [accessed Jul 30, 2017]. doi: 10.13140/RG.2.1.5193.3925

Samiksha V Vethamony P CharlsA Prasad B Balakrishnan N (2017) Wave-current interaction during Hudhud cyclone in the Bay of Bengal. *Natural Hazards Earth System Sciences* 17(12), pp.2059-2074. <https://doi.org/10.5194/nhess-17-2059-2017>

Sindhu B Unnikrishnan AS (2013) Characteristics of tides in the Bay of Bengal. *Marine Geodesy* 36(4), pp.377–407. <https://doi.org/10.1080/01490419.2013.781088>

Wessel P Smith WH Scharroo R Luis J Wobbe F (2013) Generic mapping tools: improved version released. *Eos, Transactions American Geophysical Union* 94(45), pp.409-410. <https://doi.org/10.1002/2013EO450001>

Williams J Horsburgh KJ Williams JA Proctor RN (2016) Tide and skew surge independence: New insights for flood risk. *Geophysical Research Letters*, 43(12), pp.6410-6417. <https://doi.org/10.1002/2016GL069522>

Zhang W-Z Shi F Hong H-S Shang S-P Kirby JT (2010) Tide-surge interaction intensified by the Taiwan Strait. *Journal of Geophysical Research* 115, C06012. <https://doi.org/10.1029/2009JC005762>

Zhang H Cheng W Qiu X Feng X Gong W (2017) Tide-surge interaction along the east coast of the Leizhou Peninsula, South China Sea. *Continental Shelf Research* 142, pp.32-49. <https://doi.org/10.1016/j.csr.2017.05.015>